Title
FISSION BARRIER OF THALLIUM-201

Authors
Burnett, Donald S.
Gatti, Raymond C.
Plasil, Franz
et al.

Publication Date
1963-11-27

UCRL-11079

University of California

Ernest O. Lawrence Radiation Laboratory

FISSION BARRIER OF THALLIUM-201

Berkeley, California

DISCLAIMER

UCRL-11079

UNIVERSITY OF CALIFORNIA

Lawrence Radiation Laboratory
Berkeley, California

AEC Contract No. W-7405-eng-48

FISSION BARRIER OF THALLIUM-201

Donald S. Burnett, Raymond C. Gatti, Franz Plasil, P. Buford Price,
Wladyslaw J. Swiatecki, and Stanley G. Thompson

November 27, 1963

FISSION BARRIER OF THALLIUM-201

Donald S. Burnett,* Raymond C. Gatti, Franz Plasil, P. Buford Price,**

Wladyslaw J. Swiatecki, and Stanley G. Thompson

Lawrence Radiation Laboratory
University of California
Berkeley, California

November 27, 1963

ABSTRACT

A new method involving the detection of fission fragments in mica has been applied to the measurement of the fission cross section of the compound nucleus Tl^{201} produced by bombardments of Au^{197} with helium ions. These data have been interpreted in terms of an expression for the ratio of fission to neutron-emission probabilities similar to those used conventionally, but modified to include the effect of quantum mechanical barrier penetrability. In this way a height of 22.5±1.5 MeV was found for the fission barrier of Tl^{201} and a lower limit on the width could be established. The above value of the barrier, when interpreted on the basis of the liquid drop theory, leads to an accurate determination of the ratio of the electrostatic to the surface energy of nuclei. This serves to establish the constant of proportionality between the "fissionability parameter" x and the value of Z^2/A as follows: $x = (Z^2/A)/(48.4\pm0.5)$. This measured barrier height, when added to the ground-state mass of Tl^{201}, gives a saddle-point mass of this nucleus equal to 200.9949±0.0015 mass units (carbon scale).

I. INTRODUCTION

The primary purpose of this work was determination of the fission barrier of the compound nucleus Tl^{201} produced by bombardment of Au^{197} with helium ions. The interest in reliable measurements of fission barriers is twofold. First, barrier heights are among the most fundamental and, at the same time, the simplest predictions of a theory of fission. In particular, within the framework of the liquid drop model, accurate theoretical values of relative barrier heights have become available recently.[1,2] Most of the experimental information on fission barriers has so far been confined to the heavy element region, where the barrier heights are only a few MeV, and the relative size of corrections due to shell effects is almost of the same order of magnitude.[3,4] As a result, the interpretation of the poor agreement between experiment and the simple liquid drop theory is difficult in this region of the periodic table. The situation could be clarified by an extension of barrier measurements to the lighter elements below lead, where the barrier heights are expected to increase rapidly to 20 MeV and more.

The second reason for the importance of fission barrier measurements is in connection with the determination of adjustable constants in semi-empirical mass formulae.[5] The measurement of a fission barrier, equivalent to the measurement of the mass of a nucleus in its distorted "saddle-point configuration," is potentially the most accurate way of determining the ratio of the nuclear surface tension to the electrostatic energy. The limited use made so far of fission barrier measurements in fitting constants in semi-empirical mass formulae is probably due to the inadequate understanding of fission barrier systematics in the heavy element region. A clarification by barrier measurements for lighter elements would reduce these uncertainties and would add considerably to the understanding of the systematics of nuclear masses in general.

Estimates of the fission barrier of Tl^{201} and of several other nuclei in the same region of the periodic table have been published by various authors,[6,7] most recently by Huizenga, Chaudhry, and Vandenbosch,[8] hereinafter referred to as HCV. These estimates, however, were subject to the limitation that the smallest cross sections measured were of the order of 10^{-30} cm^2. This meant that the energy of even the lowest cross-section measurement was considerably above the top of the fission barrier. Under these conditions the determination of the barrier height from the measured cross sections is very inaccurate, and the inference of finer details of the barrier, such as its thickness, is out of the question.

The possibility of improving the sensitivity and accuracy of the experimental data presented itself as a consequence of two developments. The first was in the form of a new method for the detection of fission fragments, developed by Price and Walker.[9] In this method strips of mica are used to detect the fragments. The tracks produced by fragments become easily visible under an ordinary microscope when the mica is treated with hydrofluoric acid. Background tracks from particles lighter than about mass 30 are not visible.[10] The second development came when high-intensity beams of helium ions ranging in energy from 25 to more than 120 MeV were produced by the Berkeley 88-inch variable-frequency cyclotron.[11] The width of the helium-ion energy distribution provided by this cyclotron is narrow (FWHM < 1%), and the desired values of the energies were obtained without the necessity of resorting to the use of absorber foils.

The absolute values of fission barriers calculated from experimental fission cross-section data depend, in a major way, on the formulae used to fit the data. Formulae commonly used in this connection, for example those described by HCV, are not appropriate at energies close to the fission barrier when quantum-

mechanical barrier penetration is becoming important. In the present work a suitably modified expression for the probability of fission was derived and used in the interpretation of the data.

II. EXPERIMENTAL PROCEDURE

The helium ion beams were produced by acceleration in the Berkeley 88-inch variable-energy cyclotron.[11] The beams passed through a quadrupole focusing magnet, a switching magnet, and then into the experimental area, where the beam was further focused by means of a second quadrupole magnet. The final focusing adjustments were made using, as an indicator, the light emitted from the irradiated area of a gridded quartz disc which had been placed in the position to be occupied later by the gold target. The beam passed through two graphite collimators before striking the target. The first collimator restricted the beam area to a circle of 0.25-in. diameter. The second collimator was provided with a slightly larger hole (5/16-in. diameter) in order that its edges would not be struck by the beam. The larger collimator was therefore used to shield the fission fragment detectors from any fission events that might have been produced in the first collimator.

The vacuum chamber is a copy of one described elsewhere.[12] The target and detector assembly are shown schematically in Fig. 1. After passing through the target, the beam entered a Faraday cup connected to an integrator which measured the integrated beam current. Measurements of the energies of the helium ions were made before starting the bombardments by employing the usual absorber methods. The measured values for the helium-ion energies usually agreed within 0.1 MeV with nominal values calculated for the operating conditions of the cyclotron. Although it was never essential to reduce the helium-ion energies with absorbers in order to obtain the desired energies, this method was sometimes used as a convenience--especially in order to save time. The use

of this method was restricted to the region of energies above 30 MeV, where the fission cross sections are relatively insensitive to changes in energy.

The gold targets were prepared by standard volatilization methods, using gold of the highest available purity. (Available from Cominco Products, Inc., Electronic Material Div., 933 West 3rd Ave., Spokane, Washington.) Self-supporting foils of thickness ≈ 3 mg/cm^2 were obtained, and the thickness of the foils was measured by weighing a known area. A target thickness of ≈ 3 mg/cm^2 is roughly optimum for maximum sensitivity for detection of fission fragments. If the targets are much thicker, absorption of the fragments and degradation of their energies may decrease the efficiency of detection. If the targets are much thinner, the sensitivity of the cross-section measurements would be decreased in direct proportion to the decrease in the number of atoms exposed to the beam flux. The foils were mounted on stainless steel rings of 7/8 in. inner diameter. Such a target area was chosen in order to eliminate the possibility that the helium ion beam would strike the edges of the target holder, when the target was mounted at the standard angle of 45 degrees relative to the beam direction. The gold foil was tested for the presence of natural uranium impurity by placing some of it between two sheets of mica and exposing it to a high flux of thermal neutrons. Then the mica sheets were "developed" as described below and "scanned" for fission-fragment tracks. The uranium content of these foils was found to be less than 3 parts in 10^{10} parts of gold. During the course of the preparations and throughout the experiments, special precautions were taken to insure that the possibility of contamination would be minimized.

The fission-fragment detectors were rectangular strips of mica of width 1 cm, length 1.25 cm, and convenient thickness ($\approx 10^{-2}$ cm). The strips were cleaved along layer planes in order to obtain fresh surfaces. The strips were

then pre-etched by placing them in contact with 27 M hydrofluoric acid for 2 hours at room temperature. The mica strips were removed, washed with water and alcohol, and dried. A customary inspection of the strips under a microscope shows occasional very large fission tracks (resulting from spontaneous fission of uranium impurities over long times), but the large size of these tracks makes them easily distinguishable from the smaller ones produced during the bombardments because the subsequent "developing" time with hydrofluoric acid is much shorter. Fission fragments produced in the targets enter the mica at the well-defined average angle of 30 degrees. One may therefore identify rare events originating from a location other than the target. Such background events, however, were found to be extremely rare in the experiments reported here. In final preparation for their use in each of the experiments, two mica strips were glued into a position in the aluminum V-block as illustrated in Fig. 1 and were mounted in the target assembly as indicated. In all experiments the target was mounted at 45 degrees relative to the beam direction, and the distance between the end of the block (edges of mica strips) and the target was held constant at $\approx$ 1 cm. Under these conditions, the geometry was such that roughly 7% of the total fission events produced in the target were detected.

Upon completion of the bombardments the mica detectors were soaked in 27 M hydrofluoric acid for 30 min and were washed and dried as described above. Finally the strips were mounted between two microscope cover glasses. The density of fission tracks in a "standard area" was determined by scanning under a microscope with a suitable magnification, such as 500 to 1000. The standard area refers to a strip 1.195 cm long and 0.0170 cm wide (see Fig. 1).

The number of tracks counted depended on the conditions of the experiment. Where the density of tracks was large enough, as in the case of bombardments at higher energies, a sufficient number of tracks was determined to reduce the

statistical error to a suitable value. On the other hand, at the lowest bombarding energies, relatively large areas had to be scanned in order for any tracks to be observed. In all cases the procedure was to scan first a standard strip near the center line along the length of the mica strip. In scanning along additional standard strips the same number of strips on each side adjacent to the centermost strip were scanned. This procedure was followed in order to minimize the errors due to anisotropy in the angular distributions. Reference to the angular distributions measured by Chaudhry, Vandenbosch, and Huizenga[13] shows that only in extreme cases would an error as large as 15% be made by neglecting this correction. Such extremes correspond to standard strips at the outer edges of the mica. These were scanned only in the measurements of cross sections at the lowest energies; in these cases, the statistical errors are larger than the anisotropy correction. The density of tracks along a standard strip varies by a factor of about 3 in comparing the edge of the mica closest to the target with the farthest edge. This effect is one of solid geometry.

III. RESULTS

The conditions and corresponding results of the experiments--for example, helium ion energy, number of microampere hours, number of fragment tracks observed, and density of tracks per standard strip--are given in Table I. In certain of the experiments, as indicated in the table, the energies of the helium ions were not determined by absorption measurements; in these cases the energies are listed as being uncertain from ±0.3 MeV to ±0.5 MeV (standard error). The analysis leading to this estimate of the uncertainty is based on a standard statistical analysis of the difference between the measured and calculated energies, the latter having been obtained from the stated operating conditions of the cyclotron.

The standard error listed as the uncertainty in the density of tracks per standard strip is purely statistical and does not take into account the possibility of systematic errors.

The fission cross sections given in the last column of Table I were normalized to the value 210 millibarns obtained by HCV for the same reaction with 39.6-MeV helium ions. The cross sections, σ_f, were calculated from data taken at other energies according to the relationship

$$\sigma_f = k \cdot N/I \quad ,$$

where N is the number of fission tracks per standard strip, I is the integrated beam intensity in microampere hours, and k has the value 1.77×10^{-5}, if the result is to be obtained in millibarns.

In calculating the excitation energy of the compound nucleus, corrections were made for its center-of-mass motion and for the Q value of the reaction, the latter being taken from Ref. 14 as - 1.49 MeV.

The ratio of decay probabilities, Γ_f/Γ_n, of the compound system was calculated in the usual manner (as in HCV), according to the relationship

$$\frac{\Gamma_f}{\Gamma_n} = \frac{\sigma_f}{\sigma_R} \quad , \qquad (1)$$

where σ_R is the total reaction cross section (taken for our purposes from the work of Huizenga and Igo[15]), and σ_f is the measured fission cross section. In order to check the validity of the values of σ_R used in these calculations, we compared the results obtained by means of two other computer programs available at this Laboratory for making the same calculations, and found the agreement to be within 10% over the range of particle energies from 25 to 40 MeV. The use of Eq. (1) implies neglect of the contribution to σ_f of "second chance" fission (fission following neutron emission). The correction is less than 1.5% in our

case (see HCV). Table II shows in the last column the results of calculating Γ_f/Γ_n by Eq. (1).

As mentioned previously, it was unnecessary to make any correction to the observed cross sections for the effect of beam-energy dispersion. This distribution has a Gaussian shape and a full width at half maximum of $< 1\%$. In the energy range near 25 MeV (where the fission cross sections decrease with energy by a factor of 30 per MeV) the influence of the high-energy tail of a normal distribution having the above-mentioned width would be to shift the lowest-energy points by less than 0.1 MeV.

As shown in Table I, the fission cross sections were measured at several bombarding energies above 40 MeV and data were obtained with 120-MeV helium ions. However, in order to avoid any complications resulting from fission following neutron emission, the results obtained at energies greater than 40 MeV were not used in our data analysis.

The fission cross sections as a function of excitation energy are shown in Fig. 2. The experimental cross sections range from $\approx 10^{-35}$ cm^2 up to $\approx 10^{-25}$ cm^2, an overall factor of $\approx 10^{10}$.

A plot of $\log_{10} \Gamma_f/\Gamma_n$ versus excitation energy is shown in Fig. 3. The curve drawn down through the points is the result of making least-squares fits to a newly derived theoretical expression having four parameters. The derivation of this expression is the subject of the following section of this paper. The least-squares fitting routine, basically that of Moore and Zeigler,[16] was carried out by means of an IBM 7094 computer.

IV. DERIVATION OF A FORMULA FOR Γ_f/Γ_n

The formula for Γ_f/Γ_n used in interpreting the experimental data is similar to that of HCV, with one important difference: namely, that an attempt was made to allow for the quantum-mechanical penetrability of the barrier. The resulting

expression may then be used for excitation energy above and below the barrier and, with some reservations, in the region of the barrier.

For the fission width Γ_f, we start with the expression following from the standard theory of reaction rates,[17]

$$2\pi\ \Gamma_f = N_f/\rho(E) \quad ,$$

where $\rho(E)$ is the level density in the compound nucleus at the given excitation, E, and N_f is the "effective number of open channels" at the saddle-point configuration. According to the transition-state theory a reaction rate is equal to the number of systems about to undergo disintegration in unit time (proportional to N_f) divided by the total number of nondisintegrating systems (proportional to $\rho(E)$. If barrier penetrability is disregarded, N_f is the number of energy levels associated with nonfission degrees of freedom, available to the saddle-point configuration in the range of excitation energies of the saddle configuration from zero to the maximum (given by the difference between E and the barrier height B_f). We may write this as

$$N_f = \sum_{\text{channels}} 1 \quad . \tag{2}$$

In the idealization where the level spectrum of the saddle point at excitation X is considered to be represented by a level density $\rho^*(X)$, we may replace the sum by an integral to obtain the usual formula

$$2\pi\ \Gamma_f = \frac{\int_0^{E-B_f} \rho^*(X)\,dX}{\rho(E)} \quad , \tag{3}$$

identical with Eq. (1) of HCV. Barrier penetrability is now taken into account by replacing Eq. (2) by an expression due to Wheeler (unpublished notes):

$$N_f = \sum_{\text{channels}} W \quad , \tag{4}$$

where W is the contribution of a channel, the contribution being no longer zero or unity (depending on whether one is below or above the barrier), but a gradually varying function of the position of the channel with respect to the barrier. Again following Wheeler, we take W to be given by the penetrability formula of Hill and Wheeler,[18]

$$W(T) = 1/[1 + \exp(-2\pi T/\hbar\omega)] \quad , \tag{5}$$

where T is the energy excess (in the fission degree of freedom) over the height of the barrier, for the channel in question. The relation of T to X (which is the energy in the nonfission degrees of freedom) is given by

$$E = B_f + T + X \quad .$$

This equation expresses the division at the saddle point of the total energy E into the potential and kinetic energies in the fission degrees of freedom, B_f and T, respectively, and the energy X in the nonfission degrees of freedom. The quantity $\hbar\omega$ in Eq. (5) is a measure of the thickness of the (parabolic) barrier, assumed in the derivation of the penetrability equation. (If the barrier were inverted to form a harmonic oscillator, ω would be the characteristic frequency.) Under the same idealization as before of describing the level spectrum at the saddle by a level density $\rho^*(X)$, we now find for Γ_f the expression

$$2\pi\,\Gamma_f = \frac{1}{\rho(E)} \int_0^{E(\text{or } \infty)} \rho^*(X) \frac{1}{1 + \exp[-2\pi(E - B_f - X)\hbar\omega]}\, dX \quad . \tag{6}$$

Note that the integration now extends up to X = E, since the excitation energy in the nonfission degrees of freedom may reach the full value E, provided only that the energy in the fission direction, $B_f + T$, is zero, corresponding to a negative kinetic energy $T = -B_f$, i.e., barrier penetration. The contribution to the integral from this region of the variable X is, however, damped out by the penetrability factor. For any reasonable barrier thickness this damping-

out is so rapid that it is in fact an excellent approximation to replace the upper limit by infinity. We note that as the barrier becomes very thick ($\hbar\omega \to 0$) the penetrability becomes a step function, zero below and unity above the barrier, and we recover the usual expression (3).

As regards the level densities $\rho^*(X)$ and $\rho(E)$, we have followed HCV in using the simplest version of the Fermi-gas formula,

$$\rho^*(X) = C \exp[2(a_f X)^{1/2}] \quad , \quad \rho(E) = C \exp[2(aX)^{1/2}] \quad ,$$

where C, a, and a_f are constants. With this choice the expression for Γ_f may be written as a function of E, with B_f, a, a_f and $\hbar\omega$ as parameters:

$$\Gamma_f(B_f,a,a_f,\hbar\omega;E) = \frac{(4a_f)^{-1}}{2\pi \exp[2(aE)^{1/2}]} G(\epsilon,\beta) \qquad (7)$$

where G is the following dimensionless function of two dimensionless arguments,

$$G(\epsilon,\beta) = \int_0^\infty dy\, e^{\sqrt{y}}\, 1/\{1 + \exp[(y - \epsilon)/\beta]\} \quad . \qquad (8)$$

Here ϵ is the energy excess $E - B_f$ in units of the energy defined by the quantity $(4a_f)^{-1}$, and β is proportional to the barrier thickness parameter $\hbar\omega$ in the same energy unit and y is the excitation energy X, also in units of $(4a_f)^{-1}$:

$$\epsilon = (E - B_f)/(4a_f)^{-1} \quad ,$$

$$\beta = (\hbar\omega/2\pi)/(4a_f)^{-1} \quad ,$$

$$y = X/(4a_f)^{-1} \quad .$$

When $\beta \to 0$, the integral may be evaluated explicitly, $G(\epsilon,0) = [(\sqrt{\epsilon} - 1)e^{\sqrt{\epsilon}} + 1]$. Various approximations to $G(\epsilon,\beta)$ may be developed for small or large values of the arguments, but in the work reported here $G(\epsilon,\beta)$ was evaluated by numerical integration with the aid of an electronic computer. The following properties of $G(\epsilon,\beta)$ may be noted. The integrand in (8) represents the competition between

two factors, the level density $e^{\sqrt{y}}$, which favors large excitations, and the penetrability, which favors small excitations. The maximum in the integrand occurs when y has the value given by

$$2\sqrt{y}/\beta = 1 + \exp[-(y - \epsilon)/\beta] \quad . \tag{9}$$

For example, if the maximum is to correspond to processes just grazing the barrier ($y - \epsilon = 0$), we find from Eq. (9) that the condition on the energy E is given by

$$y = \beta^2 \quad ,$$

or

$$E - B_f = (\hbar\omega/2\pi)^2/(4a_f)^{-1} \quad .$$

Taking $\hbar\omega = 1$ MeV, $a_f = 16.4$ MeV^{-1} as an illustration, we find that $E - B_f = 2$ MeV. Thus the energy has to exceed the barrier by 2 MeV before the most probable process proceeds over rather than through the barrier. A plot of the integrand for this choice of parameters is shown in Fig. 4. Similarly we find that when the energy, E, is just equal to the barrier height, B_f, then, in the above example, the most probable process penetrates the barrier 0.5 MeV below the top.

When E is well below the barrier, so that $e^{(y-\epsilon)/\beta} \gg 1$, the function $G(\epsilon,\beta)$ reduces to

$$G(\epsilon,\beta) \longrightarrow e^{\epsilon/\beta}\,\beta\{1 + (\sqrt{\pi}/2)e^{\beta/4}\sqrt{\beta}[1 + \mathrm{erf}(\sqrt{\beta}/2)]\} \quad , \tag{10}$$

which corresponds to a fission width decreasing with energy as a simple exponential at a rate characteristic of the barrier thickness. (The energy dependence is given by the factor $e^{\epsilon/\beta}$, equal to $\exp[(E - B_f)/(\hbar\omega/2\pi)]$.)

For the neutron width, Γ_n, we used the same expression as HCV. It results from applying Eq. (3) to the case of neutron emission. The transition state is now the configuration of the residual nucleus with the neutron just outside

its surface. The level density ρ^* of this configuration may be written as a product of the level density $\rho^{**}(x)$ of the residual nucleus at excitation x and the density of appropriate levels for the neutron, which turns out to be proportional to the neutron's kinetic energy, t, given by $t = E - B_n - x$ (see Bohr and Wheeler[17]). B_n is the binding energy of the neutron. The result is

$$2\pi\,\Gamma_n = 2\left[\int_0^{E-B_n} dx\;\rho^{**}(x)(t/t_o)\right]/\rho(E) \quad , \tag{11}$$

where $t_o = \hbar^2/2mR^2$, m is the neutron mass, and R is the radius of the residual nucleus. The factor 2 is associated with the two directions of the neutron spin. Using for ρ^{**} the approximation $C\exp[2(a_n x)^{1/2}]$ the integral can again be evaluated explicitly. The final expression for the ratio Γ_f/Γ_n may be written as

$$\frac{\Gamma_f}{\Gamma_n} = \frac{a_n^2 t_o}{a_f}\,G(\epsilon,\beta)/\{e^{\sqrt{\eta}}(2\eta - 6\sqrt{\eta} + 6) - 6 + \eta\} \quad , \tag{12}$$

where $\eta = (E - B_n)/(4a_n)^{-1}$. We used the value 11.37 MeV for t_o. The principal limitation of our formula for Γ_f is probably the neglect of the discreteness at the saddle point of the energy levels, which are treated in terms of a continuous level density $\rho^*(X)$. This idealization would appear to be always a good approximation at high energies, when the relevant channel spacing is small. At energies close to or below the barrier, when the dominant channels are not closely spaced, the formula might still be a good approximation for sufficiently thin barriers, for which $\hbar\omega$ is much greater than the level spacing, since this condition ensures the simultaneous contribution of many channels to the fission cross section. If this condition is not satisfied (low energies, thick barriers), the fission cross section for energies close to the top of the barrier would be expected to show fluctuations associated with the discreteness of the channels.[19] In such cases our formula represents some average over such oscillations, connecting in a smooth way the exponential behavior of the cross section well below the barrier and the smooth increase well above the barrier.

V. DISCUSSION

The comparison of the experimental measurements with formula (12) proceeded in several stages. First, all the parameters B_f, a_f, a_n, and $\hbar\omega$ were assigned fixed values which seemed of a reasonable magnitude from known or estimated properties of nuclei. Thus, $B_f = 27.2$ MeV follows from a liquid drop barrier corrected for shell effects (an extra stability of the ground state of about 4.3 MeV). Green's parameters were used in the liquid drop formula for the surface and electrostatic energies. The values $a_f = a_n = 22.5$ are a little below the 25 suggested by the rough rule $a = A/8$.[21]

Estimates of $\hbar\omega$ suggested that this quantity could be a rather sensitive function of the position of the nucleus in the periodic table, tending from low values for heavy elements to high values for light elements. (We are indebted to Mr. James Rayford Nix for help with estimating $\hbar\omega$.) A range of values of $\hbar\omega$, usually from 0 to 4 MeV, was considered in the comparisons.

Figure 5 shows the result of inserting the above parameters in Eq. (12). We note that the absolute values of Γ_f/Γ_n are many orders of magnitude too small. (This figure illustrates well the influence of the barrier thickness on Γ_f/Γ_n. The effect of penetrability is of course all-important below the barrier, but may also be considerable at the barrier and for several MeV above.)

The next stage, illustrated by Fig. 6, shows the effect of relaxing the requirement that a_n should be close to $A/8$, since it is known that nuclei in the neighborhood of closed shells (such as Tl^{200}) are characterized by smaller values of this parameter.[20] The values of a_n were adjusted to make all the curves pass through the same point at $E = 30$ MeV. We see that with values of a_n about 10, the order of magnitude of Γ_f/Γ_n can now be reproduced at a given energy but that the slope and shape of the calculated curves are still quite incorrect. In Fig. 7, the value of B_f instead of a_n was varied arbitrarily,

since some uncertainty exists in the calculated value of B_f, mainly on account of possible changes in the parameters of the surface and Coulomb energies in the semi-empirical mass formula. We see that decreasing B_f alone can again make Γ_f/Γ_n come up to the right order of magnitude for a given energy, but the slope of the curves is too small.

Concluding that at least two parameters must be allowed to vary simultaneously, we have prepared Fig. 8, where only a_f is fixed at 22.5 and a_n and B_f are varied. (Our preference for keeping a_f near A/8 resulted from the belief that shell effects would be less likely at the saddle-point configuration.) The curves in Fig. 8 were all made to pass through two points, at 30 and 37 MeV. We see that the slope as well as the magnitude of the experimental curve is now reproduced over part of the range of energies, but for no choice of $\hbar\omega$ can a satisfactory fit be found over the whole range. (A preference for low values of $\hbar\omega$ is beginning to emerge.)

It seems necessary, then, to vary all the parameters, and this was done in Fig. 9, where all curves were fitted to three points, at 23, 30, and 37 MeV. Completely satisfactory fits become possible at once provided $\hbar\omega$ is not too large (in the neighborhood of 0 to 1 MeV). The above analysis indicates, then, that the experimental points cover a sufficient range in energy and cross section and provide a curve with sufficient structure to determine four parameters in Eq. (12). The absolute magnitude, slope, and curvature of the experimental curve determine the values of B_f, a_n, and a_f, and a further shape characteristic, related to the third derivative (an increase of curvature at low energies), serves to put limits on $\hbar\omega$. With this in mind, we made least-squares fits to the data for a series of fixed values of $\hbar\omega$ ranging from 0 to 3 MeV; the results are shown in Figs. 10 and 11. (A measure of the goodness of the fit is the values of ψ^2, which is the sum of the squares of the differences

between the measured and calculated values of $\log_{10} \Gamma_f/\Gamma_n$. The values of ψ^2 associated with the fits obtained under various conditions are given in the tables shown in Figs. 10, 11, and 12.)

We see that about equally good fits may be obtained for any value of $\hbar\omega$ between 0 and 1 MeV, with values of a_f and a_n in the neighborhood of 17 and 13. The values of B_f range from 22.1 to 22.5 MeV. The fits for $\hbar\omega$ up to 2 MeV, though not quite as good, are acceptable, but they require a_f and a_n to be lowered to about 10 and 7.5, respectively. For $\hbar\omega = 3$ (Fig. 10), a good fit to the data cannot be found for any choice of B_f, a_f, and a_n, and the best fit, shown in Fig. 10, requires quite unreasonable values of a_f and a_n (3.7 and 2.8, respectively). In other words, for excessively large values of $\hbar\omega$--a very thin barrier--it is impossible to reproduce the steepness of the experimental curve around $E = 23$ to 24 MeV. (In our analysis we have treated the two points at the lowest energies on an equal footing with the rest of the data, although they are based on only three observed events each. The significance of these points is greater than the low number of counts would indicate in that they serve to put an upper limit on the contaminations present in the foil. The conclusions of this section would not be changed significantly if these points were treated only as upper limits rather than actual values of Γ_f/Γ_n.)

With this understanding of the role of the parameter $\hbar\omega$, we finally proceeded to an analysis of the data designed to bring out the best value to be adopted for the barrier, B_f. Figure 12 and the accompanying table show the effect of assuming B_f to be 18, 19, ... MeV, and adjusting the remaining parameters for a best fit. For B_f up to 22 MeV the best fit is obtained by taking $\hbar\omega$ exactly zero. For $B_f > 22.5$ MeV finite values of $\hbar\omega$ are called for. The best fits, as judged by the sum of the squares of the deviations, are found in the neighborhood of $B_f = 22$ or 23 MeV, with $\hbar\omega$ between 0 and 1.4 MeV, and the

pair a_f, a_n between 18.9,14.0 and 14.3,10.6. We note the steep dependence of a_f and a_n on the assumed B_f. For B_f less than 21 MeV or greater than 24 MeV the values of a_f and a_n required for a fit begin to be unreasonable, and this could be used in conjunction with the deteriorating representation of the data to exclude such values of B_f.

The value of B_f we shall adopt is $B_f = 22.5 \pm 1.5$ MeV, the indicated uncertainty reflecting in part the requirement that a_f and a_n should stay within reasonable bounds. Similarly the indicated value of $\hbar\omega$ is in the range 0 to 2.

The value 22.5±1.5 MeV for the barrier B_f is 2.6 MeV higher than the 19.9±2 MeV estimated by HCV from cross-section measurements that start about .4 MeV higher in energy than ours, where the value of Γ_f/Γ_n has increased by about four orders of magnitude. As regards the level density parameters a_f and a_n, we confirm the results of HCV in showing that, for any acceptable fit, a_f is larger than a_n, the ratio being remarkably close to 1.35 (within 1% for all except very poor fits). From the tables associated with Figs. 10, 11, and 12, we see that the highest values of a_f and a_n are obtained with the smallest values of $\hbar\omega$ and the smallest values of B_f. A value of a_f consistent with a rough rule such as $a = A/8$ could be made to satisfy the experimental data, if the barrier, B_f, were chosen to be between 21 and 22 MeV and a small value of $\hbar\omega$ were used (see Fig. 12). The somewhat lower values of a_n may reflect the proximity of the residual nucleus Tl^{200} to the closed shell at Pb^{208} (Fig. 1 of Reference 20). The value of a_f, characteristic of the saddle-point configuration, is not expected to be affected by this shell.

[We tried to develop a simple theory of the effect of shells on nuclear level densities but, after some unsuccessful attempts, we stayed with the simplest Fermi gas expression for the level density, shell effects being

accommodated in an ill-defined manner by allowing a_n and a_f to be adjustable parameters (instead of being fixed constants, determined by the density and composition of the Fermi gas). The result is that we cannot be sure about the significance of the limits ± 1.5 MeV placed on the value of the barrier B_f.]

We have neglected in our analysis the effects resulting from the angular momentum brought into the nucleus by the helium ions. At the lower range of energies in our measurements (the range that is most important for the determination of the fission barriers), the α particle is only a few MeV above the Coulomb barrier and brings in less than 10 units of angular momentum (a maximum of 8.5 units at a bombarding energy of 25 MeV). Using data from Reference 21, we estimate that the error in our estimate of B_f resulting from the neglect of angular momentum effects is not more than a few tenths MeV.

Accepting the value $B_f = 22.5 \pm 1.5$ MeV for the fission barrier of Tl^{201}, we shall deduce the ratio of the electrostatic energy to the surface energy for this nucleus--or, equivalently, the value of the fissionability parameter, x, defined as

$$x = \frac{(\text{charge})^2}{10(\text{volume})(\text{surface tension})}$$

$$= \frac{(\text{electrostatic energy of sphere})}{2(\text{surface energy of sphere})}$$

$$= (Z^2/A)/(Z^2/A)_{\text{critical}}, \text{ for a nucleus idealized as a charged drop.}$$

We estimate that of the 22.5±1.5 MeV, the amount of 4.3 MeV is due to the extra stability of the ground state of Tl^{201} (Reference 5), leaving 18.2±1.5 MeV to be accounted for by the increase in the sum of surface and electrostatic energies in the saddle-point configuration of the nucleus. According to the liquid drop model, this energy increase may be written in units of the surface energy, $a_2A^{2/3}$, as

$$B_f = a_2A^{2/3}\xi(x) \quad , \tag{12a}$$

or, in units of the electrostatic energy, $a_3 \frac{Z^2}{A^{1/3}}$, as

$$B_f = a_3 \frac{Z^2}{A^{1/3}} \frac{\xi(x)}{2x} \quad . \qquad (12b)$$

Here $\xi(x)$ is a known dimensionless function of x (see Cohen and Swiatecki[2]).

Taking Green's value, 17.80 MeV, for the surface energy coefficient a_2, we find the ratio $B_f/a_2A^{2/3} = (18.2\pm1.5)/17.80\ A^{2/3} = 0.0298\pm0.0025$. From Eq. (12a) and Reference 2, we then obtain

$$x(Tl^{201}) = 0.675\pm0.013$$

and, consequently,

$$(Z^2/A)_{crit} = 48.4\pm0.5 \quad .$$

Had we used Green's value of the electrostatic energy coefficient $a_3 = 0.710$ MeV and Eq. (12b), we would have found instead $x(Tl^{201}) = 0.672$ and $(Z^2/A)_{crit} = 48.6$. The values of $x(Tl^{201})$ and $(Z^2/A)_{crit}$ required to reproduce the experimental barrier for Tl^{201} are quite insensitive to the absolute values of a_2 or a_3. Thus, increasing a_3 by 5% to 0.746 MeV, leads to $x(Tl^{201}) = 0.676$, $(Z^2/A)_{crit} = 48.3$, a change of about half a percent. This is a consequence of the sensitivity of the barrier, B_f, to the value of the fissionability parameter, x. One may thus determine the ratio of the electrostatic to the surface energy rather precisely even in the absence of an accurate absolute determination of either quantity. As a result, we may adopt with some confidence the following equation for calculating the fissionability parameter for a nucleus idealized as a charged drop,

$$x = (Z^2/A)/(48.4\pm0.5) \quad .$$

This relation may be regarded as a consequence of interpreting our barrier measurement, $B_f = 22.5\pm1.5$ MeV, in terms of the liquid drop model. Another way

of stating our result, which is independent of the assumption of this model, is that we have determined the mass of the Tl^{201} nucleus in that (saddle-point) configuration where the cohesive and disruptive forces are just balanced in unstable equilibrium. This mass is equal to the ground-state mass of Tl^{201} (Reference 14) plus 22.5 MeV, or

$$M_{\text{saddle-point}}(Tl^{201}) = 200.9949 \pm 0.0015 \text{ mass units on the carbon scale.}$$

An adequate semi-empirical mass formula ought to reproduce this saddle-point mass as well as the ground-state masses of nuclei.

VI. CONCLUSIONS

A new method involving the detection of fission fragments in mica has been applied to the measurement of the fission cross section of the compound nucleus Tl^{201} produced by bombardments of Au^{197} with helium ions. These data have been interpreted in terms of an expression for Γ_f/Γ_n having four adjustable parameters which include a fission barrier thickness parameter $\hbar\omega$. The results are that the fission barrier of Tl^{201} is 22.5±1.5 MeV and the value of $\hbar\omega$ is in the range 0.0 to about 2 MeV. The values of the level density parameters obtained are $a_f \approx 16$ and $a_n \approx 12$, with large uncertainties. The value of $(Z^2/A)_{\text{limiting}}$ calculated from the above-mentioned barrier estimate is 48.4±0.5, which is within about a half a unit of the first estimate of Bohr and Wheeler.

ACKNOWLEDGMENTS

The work of adopting the least-squares fitting program to the theoretical functions, data fitting proper, and all activities directly concerned with the computers were carried out by Claudette Rugge. Her outstanding contribution to this work deserves the highest recognition.

We are grateful to Bernard G. Harvey and the staff of the 88-inch cyclotron for help and cooperation with the experimental work. We also acknowledge the

valuable assistance of Jean Rees and Joan Phillips in preparing this manuscript and in helping with the scanning. We are grateful to Ray Nix and John Huizenga for very valuable discussions. We appreciate the support given by the General Electric Company in enabling one of us (Price) to take part in these experiments.

This work was done under the auspices of the U. S. Atomic Energy Commission.

FOOTNOTES AND REFERENCES

*Now at General Electric Company, Schenectedy, New York.

**Now at Kellogg Radiation Laboratory, California Institute of Technology, Pasadena, California.

1. V. M. Strutinski, N. Ya Lyashchenko, and N. A. Popov, Soviet Phys.-JETP 16, 418 (1963).
2. S. Cohen and W. J. Swiatecki, Ann. Phys. N.Y. 22, 406 (1963).
3. W. J. Swiatecki, Phys. Rev. 101, 97 (1956).
4. Sven A. E. Johansson, Nucl. Phys. 22, 529-552 (1961).
5. W. J. Swiatecki, Semi-Empirical Interpretation of Nuclear Masses and Deformations(Talk presented at the Vienna Conference on Nuclear Masses, Aug. 1963).
6. I. Halpern, Ann. Rev. Nucl. Sci. 9, 245 (1959).
7. Earl K. Hyde, A Review of Nuclear Fission, Part I - Fission Phenomena at Low Energy, Lawrence Radiation Laboratory Report UCRL-9036, March 1960 (unpublished).
8. J. R. Huizenga, R. Chaudhry, and R. Vandenbosch, Phys. Rev. 126, 210-219 (1962).
9. P. B. Price and R. M. Walker, J. Appl. Phys. 33, 2625-2628 (1962).
10. R. L. Fleischer, E. L. Hubbard, P. B. Price, and R. M. Walker, Phys. Rev. (to be published).
11. Elmer L. Kelly, General Description and Operating Characteristics of the Berkeley 88-Inch Cyclotron, Lawrence Radiation Laboratory Report UCRL-10081, April 1962.
12. T. Sikkeland, E. L. Haines, and V. E. Viola, Phys. Rev. 125, 1350 (1962).
13. R. Chaudhry, R. Vandenbosch, and J. R. Huizenga, Phys. Rev. 126, 220-227 (1962).

14. L. A. König and J. H. E. Mattauch, Nucl. Phys. 31, 18-42 (1962).

15. J. R. Huizenga and G. J. Igo, Nucl. Phys. 29, 462 (1962).

16. R. H. Moore and R. K. Zeigler, Los Alamos Report 2367, 1960 (unpublished).

17. Niels Bohr and John Archibald Wheeler, Phys. Rev. 56, 426-450 (1939).

18. David Lawrence Hill and John Archibald Wheeler, Phys. Rev. 89, 1102-1145 (1953).

19. J. A. Wheeler, Record of Proceedings of Session 7A, August 11, 1955, Proceedings of the International Conference on the Peaceful Uses of Atomic Energy, II, United Nations, New York, 220-224, 1956.

20. E. Erba, U. Facchini, and E. Saetta Menichella, Nuovo Cimento 22, 1237-1260 (1961).

21. S. Cohen, F. Plasil, and W. J. Swiatecki, The Deformation Energy of a Rotating Charged Drop (in preparation).

Table I. Experimental data.

Helium ion energy (MeV)		Tl^{201} excitation energy, E_x (MeV)	Bombardment (μA hours)	Total fission events observed	Number of standard strips	Fission events per standard strip	Fission cross section (cm^2)
Calculated*	Measured						
-	24.9±0.1	22.9±0.1	43.77	3	47	0.0638± 0.0369	$2.60\pm1.49 \times 10^{-35}$
-	25.1±0.1	23.1±0.1	19.00	3	57	0.0527± 0.0304	$4.92\pm2.84 \times 10^{-35}$
-	25.8±0.1	23.8±0.1	28.00	51	29	1.76 ± 0.24	$1.12\pm0.15 \times 10^{-33}$
-	26.5±0.1	24.5±0.1	5.7	40	55	0.73 ± 0.11	$2.27\pm0.33 \times 10^{-33}$
-	27.0±0.1	25.0±0.1	1.5	28	54	0.519 ± 0.098	$6.14\pm1.16 \times 10^{-33}$
-	27.8±0.1	25.8±0.1	6.01	196	14	14.0 ± 1.0	$4.14\pm0.30 \times 10^{-32}$
29.0±0.3	-	26.9±0.3	3.018	298	11	27.0 ± 1.6	$1.59\pm0.09 \times 10^{-31}$
29.7±0.3†	-	27.6±0.3	1.256	126	5	25.2 ± 2.2	$3.56\pm0.31 \times 10^{-31}$
-	30.5±0.1	28.4±0.1	0.80	70	3	22.3 ± 2.68	$4.95\pm0.60 \times 10^{-31}$
30.8±0.3†	-	28.7±0.3	0.703	142	5	28.4 ± 2.4	$7.17\pm0.60 \times 10^{-31}$
-	31.6±0.1†	29.5±0.1	1.0874	495	3	165 ± 7	$2.69\pm0.12 \times 10^{-30}$
-	32.9±0.1	30.8±0.1	0.9192	653	2	326.5 ±12.5	$6.30\pm0.24 \times 10^{-30}$
33.0±0.3	-	30.8±0.3	0.35	278	2	139.0 ± 8.3	$7.05\pm0.42 \times 10^{-30}$
-	33.8±0.1†	31.6±0.1	0.3088	562	3	187 ± 8	$1.07\pm0.05 \times 10^{-29}$
35.2±0.3†	-	33.0±0.3	0.1957	939	3	313 ±10	$2.84\pm0.09 \times 10^{-29}$
37.4±0.3†	-	35.2±0.3	0.2003	732	0.61	1200 ±54	$1.06\pm0.05 \times 10^{-28}$
-	39.5±0.1	37.2±0.1	0.2015	4690	3	1563 ±23	$1.38\pm0.20 \times 10^{-28}$
39.6±0.3	-	37.2±0.3	0.2001	2368	1	2368 ±49	$2.10\pm0.03 \times 10^{-28}$**
50.4±0.4†	-	47.9±0.4	0.0151	6353	3.04	2090 ±26.2	$2.46\pm0.03 \times 10^{-27}$
51.1±0.4†	-	48.6±0.4	0.015	4099	2.05	2000 ±31.2	$2.17\pm0.03 \times 10^{-27}$
58.9±0.4†	-	56.2±0.4	0.0152	6206	0.76	8166 ±104	$9.47\pm0.12 \times 10^{-27}$
61.5±0.4†	-	58.8±0.4	0.004	4772	2.11	2262 ±32.7	$9.19\pm0.14 \times 10^{-27}$
66.5±0.4	-	63.7±0.4	0.002	4233	2.11	2006 ±30.8	$1.63\pm0.03 \times 10^{-26}$
92.9±0.5†	-	89.5±0.5	0.00105	13882	2.08	6674 ±56.6	$9.40\pm0.08 \times 10^{-26}$
119.7±0.5†	-	115.8±0.5	0.000114	5041	3.03	1664 ±23.4	$2.16\pm0.03 \times 10^{-25}$

* Nominal, based on operating conditions of cyclotron.

† Energy obtained by degrading with absorbers.

** The value normalized to HCV.

Table II. Results of the experiments.

Tl^{201} excitation energy, E_x (MeV)	Measured fission cross section, σ_f (cm^2)	Calculated reaction cross section, σ_R (cm^2)(Ref. 15)	Γ_f/Γ (σ_f/σ_R^n)
22.9±0.1	$2.60\pm1.49 \times 10^{-35}$	6.78×10^{-25}	$3.83\pm2.20 \times 10^{-11}$
23.1±0.1	$4.92\pm2.84 \times 10^{-35}$	6.87×10^{-25}	$7.16\pm4.13 \times 10^{-11}$
23.8±0.1	$1.12\pm0.15 \times 10^{-33}$	7.92×10^{-25}	$1.41\pm0.19 \times 10^{-9}$
24.5±0.1	$2.27\pm0.33 \times 10^{-33}$	8.53×10^{-25}	$2.66\pm0.39 \times 10^{-9}$
25.0±0.1	$6.14\pm1.16 \times 10^{-33}$	9.05×10^{-25}	$6.78\pm1.28 \times 10^{-9}$
25.8±0.1	$4.14\pm0.30 \times 10^{-32}$	9.85×10^{-25}	$4.20\pm0.30 \times 10^{-8}$
26.9±0.3	$1.59\pm0.09 \times 10^{-31}$	1.08×10^{-24}	$1.47\pm0.08 \times 10^{-7}$
27.6±0.3	$3.51\pm0.31 \times 10^{-31}$	1.15×10^{-24}	$3.10\pm0.27 \times 10^{-7}$
28.4±0.1	$4.95\pm0.60 \times 10^{-31}$	1.21×10^{-24}	$4.09\pm0.50 \times 10^{-7}$
28.7±0.3	$7.17\pm0.60 \times 10^{-31}$	1.24×10^{-24}	$5.78\pm0.48 \times 10^{-7}$
29.5±0.1	$2.69\pm0.12 \times 10^{-30}$	1.28×10^{-24}	$2.10\pm0.09 \times 10^{-6}$
30.8±0.1	$6.30\pm0.24 \times 10^{-30}$	1.38×10^{-24}	$4.57\pm0.17 \times 10^{-6}$
30.8±0.3	$7.05\pm0.42 \times 10^{-30}$	1.39×10^{-24}	$5.07\pm0.30 \times 10^{-6}$
31.6±0.1	$1.07\pm0.05 \times 10^{-29}$	1.44×10^{-24}	$7.43\pm0.32 \times 10^{-6}$
33.0±0.3	$2.84\pm0.09 \times 10^{-29}$	1.52×10^{-24}	$1.87\pm0.06 \times 10^{-5}$
35.2±0.3	$1.06\pm0.05 \times 10^{-28}$	1.65×10^{-24}	$6.42\pm0.29 \times 10^{-5}$
37.2±0.1	$1.38\pm0.20 \times 10^{-28}$	1.73×10^{-24}	$7.98\pm0.12 \times 10^{-5}$
37.2±0.3	$2.10\pm0.03 \times 10^{-28}$	1.73×10^{-24}	$1.21\pm0.02 \times 10^{-4}$

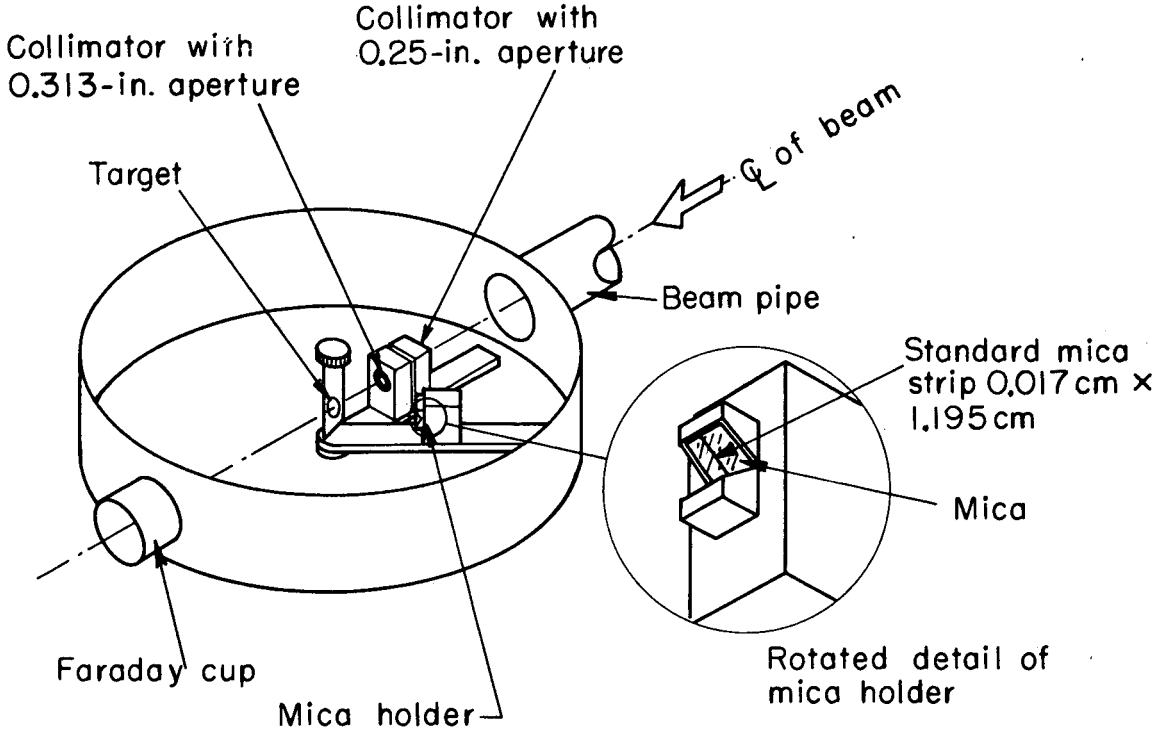
Collimator with
0.313-in. aperture
Collimator with
0.25-in. aperture
Target
℄ of beam
Beam pipe
Standard mica
strip 0.017 cm ×
1.195 cm
Mica
Faraday cup
Mica holder
Rotated detail of
mica holder

MU-32961

Fig. 2. Measured fission cross section versus excitation energy for the reaction $_{79}Au^{197} + _{2}He^{4} \rightarrow _{81}Tl^{201}$.

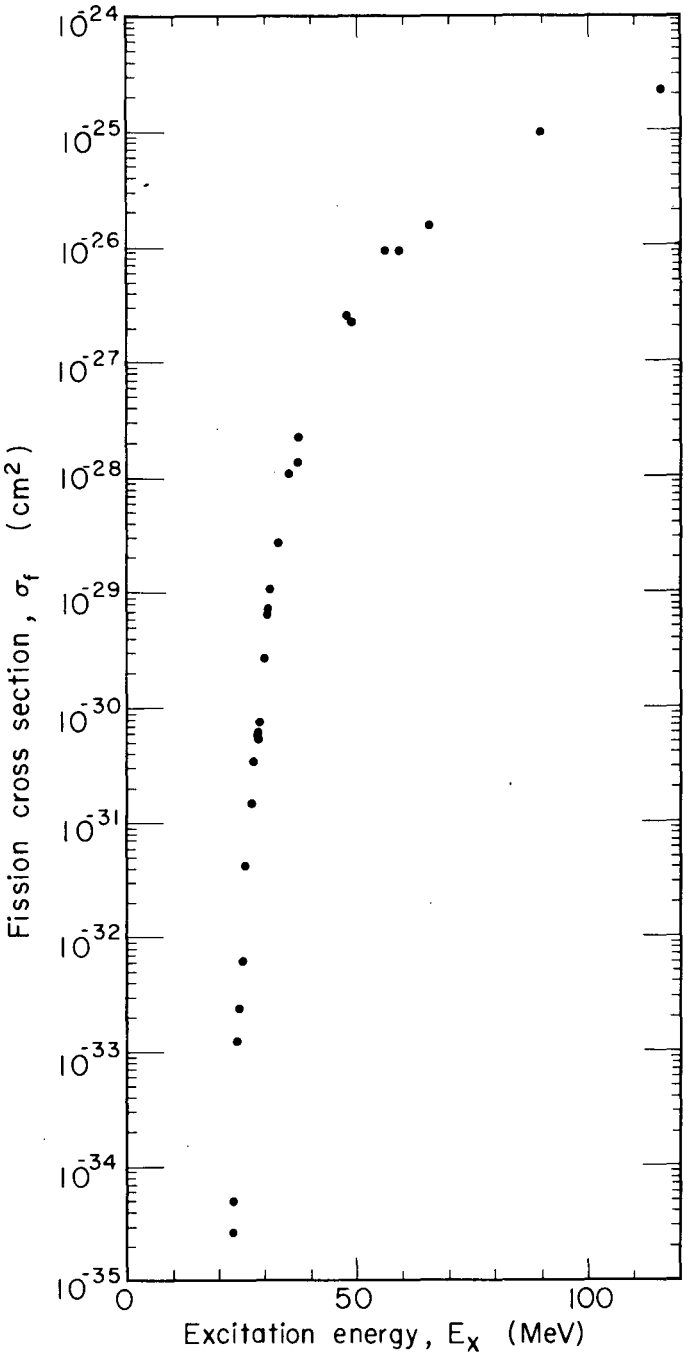
Fission cross section, σ_f (cm^2)
10^{-24}
10^{-25}
10^{-26}
10^{-27}
10^{-28}
10^{-29}
10^{-30}
10^{-31}
10^{-32}
10^{-33}
10^{-34}
10^{-35}
0
50
100
Excitation energy, E_x (MeV)

MUB-2301

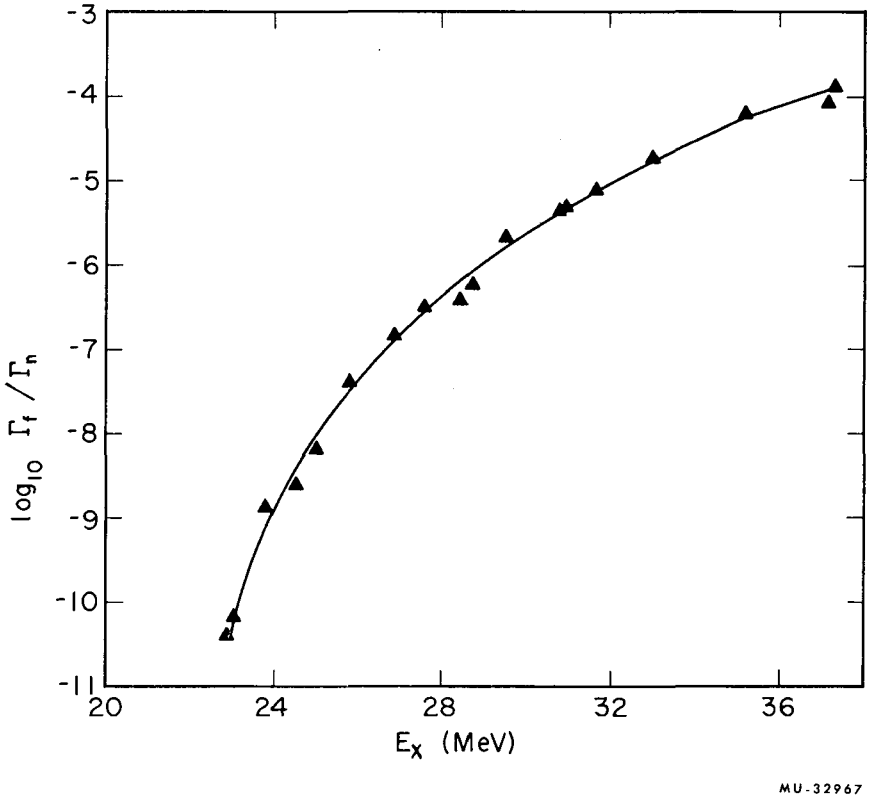
-3
-4
-5
-6
-7
-8
-9
-10
-11
$\log_{10} \Gamma_f / \Gamma_n$
20
24
28
32
36
E_x (MeV)
MU-32967

Fig. 4. A plot of the integrand in Eq. (9) as a function of the excitation energy (scale labeled X) or the kinetic energy in the fission degree of freedom (scale labeled T). For the choice of parameters indicated ($E_f = 22.5$, $\hbar\omega = 1$, $a_f = 16.4$, $E = 24.5$; $X = y/4a_f$, $T = E - B_f - X$), the maximum in the curve occurs close to $T = 0$, corresponding to events that graze the top of the fission barrier.

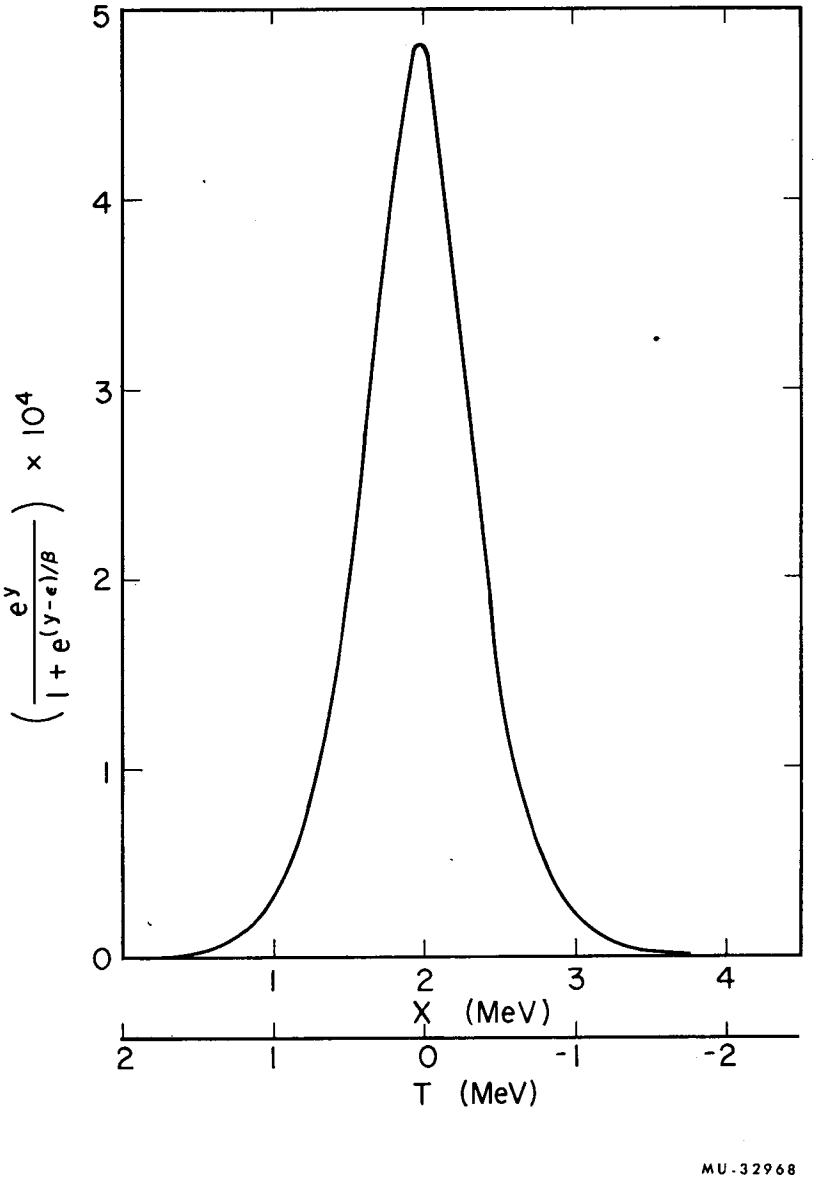
5
4
3
2
1
0
$\left(\frac{e^y}{1+e^{(y-\epsilon)/\beta}}\right) \times 10^4$
1
2
3
4
X (MeV)
2
1
0
-1
-2
T (MeV)
MU-32968

Fig. 5. Dependence of $\log_{10} \Gamma_f/\Gamma_n$ on excitation energy for various assumed values of the barrier penetrability factor, $\hbar\omega$, taking $B_f = 27.2$ MeV and $a_n = a_f = 22.5$ MeV^{-1}. Experimental points are indicated by triangles. The calculated values of Γ_f/Γ_n are many orders of magnitude too small.

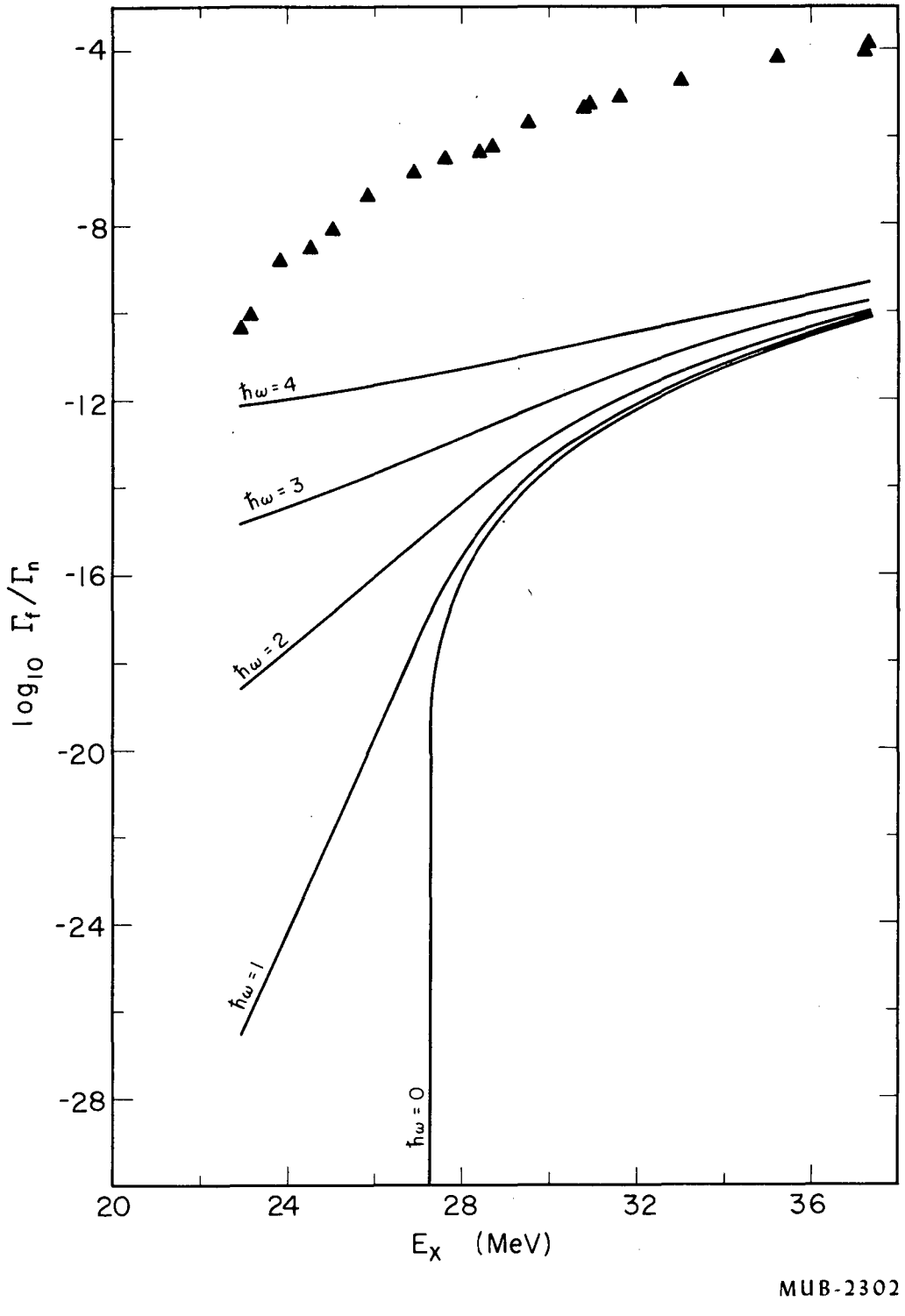
-4
-8
-12
-16
-20
-24
-28
$\log_{10} \Gamma_f/\Gamma_n$
$\hbar\omega = 4$
$\hbar\omega = 3$
$\hbar\omega = 2$
$\hbar\omega = 1$
$\hbar\omega = 0$
20
24
28
32
36
E_x (MeV)
MUB-2302

$\hbar\omega$ (MeV)	a_n (MeV^{-1})
0	6.96
1	7.26
2	7.99
3	9.31
4	11.2

Fig. 6. The dependence of $\log_{10} \Gamma_f/\Gamma_n$ on excitation energy with B_f fixed at 27.2 MeV, and a_f fixed at 22.5 MeV^{-1}. The parameter a_n was allowed to vary in order to fit the measurements at 30 MeV. The calculated values of $\log_{10} \Gamma_f/\Gamma_n$ vs excitation energy are shown for various assumed values for the barrier penetrability factor, $\hbar\omega$. The experimental points are indicated by triangles. The slope and shape of the calculated curves are incorrect.

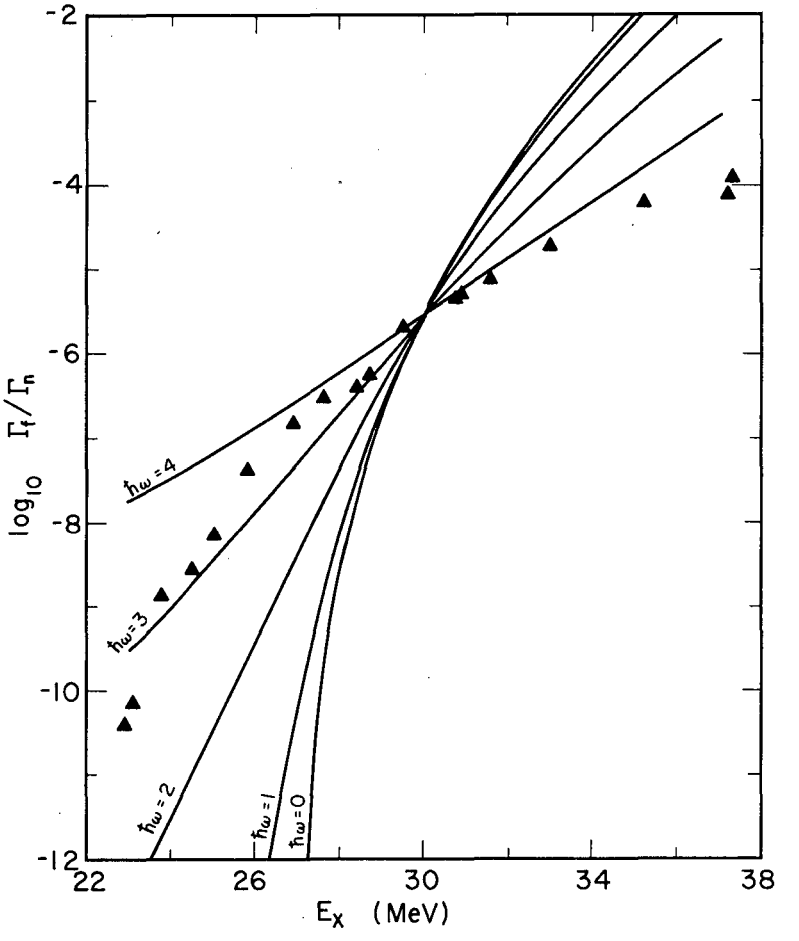
-2
-4
-6
-8
-10
-12
log10 Γf/Γn
ħω=4
ħω=3
ħω=2
ħω=1
ħω=0
22
26
30
34
38
Ex (MeV)
MU-32969

$\hbar\omega$ (MeV)	B_f (MeV)
0	17.5
1	17.6
2	17.8
3	18.1
4	18.7

Fig. 7. The effect of allowing B_f to vary in order to obtain a fit to the measurements at 30 MeV while maintaining $a_f = a_n = 22.5$ MeV^{-1}. The dependence of the calculated values of $\log_{10} \Gamma_f/\Gamma_n$ on excitation energy are shown for various assumed values of $\hbar\omega$. The measured points are indicated by triangles. The slope of the calculated curves is too small.

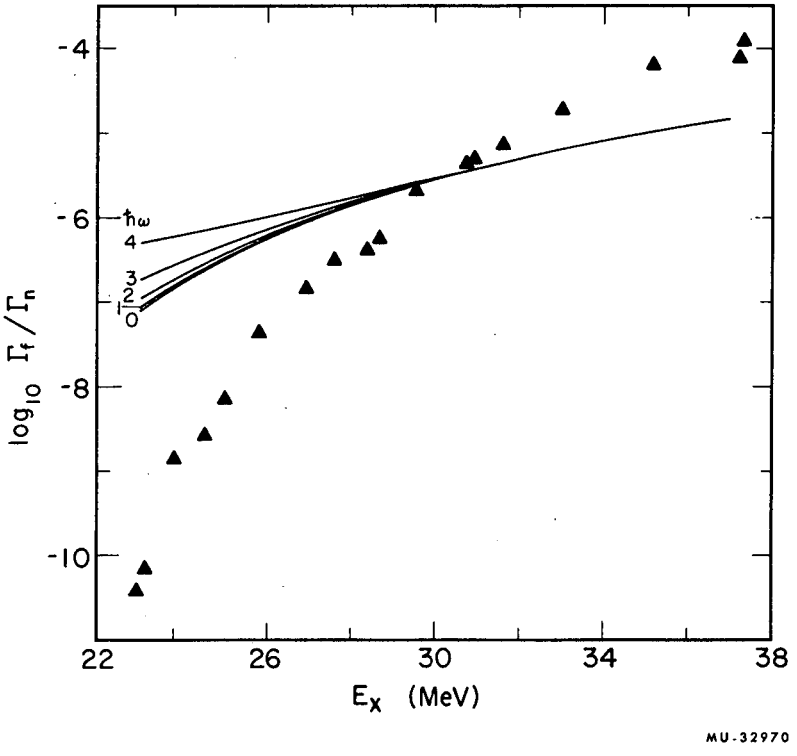
-4
-6
-8
-10
$\log_{10} \Gamma_f / \Gamma_n$
$\hbar\omega$
4
3
2
0
22
26
30
34
38
E_x (MeV)
MU-32970

$\hbar\omega$ (MeV)	B_f (MeV)	a_n (MeV^{-1})
0	20.8	17.5
1	20.9	17.5
2	21.3	17.3
3	22.0	16.9

Fig. 8. The effect of fixing a_f at 22.5 MeV^{-1} and allowing a_n and B_f to vary in such a way as to fit the measurements at 30 MeV and 37 MeV. The dependence of the calculated values of $\log_{10} \Gamma_f/\Gamma_n$ on excitation energy are shown for various assumed values of $\hbar\omega$. The measured points are indicated by triangles. The slope and magnitude of the calculated curves reproduce the measurements in the high-energy region.

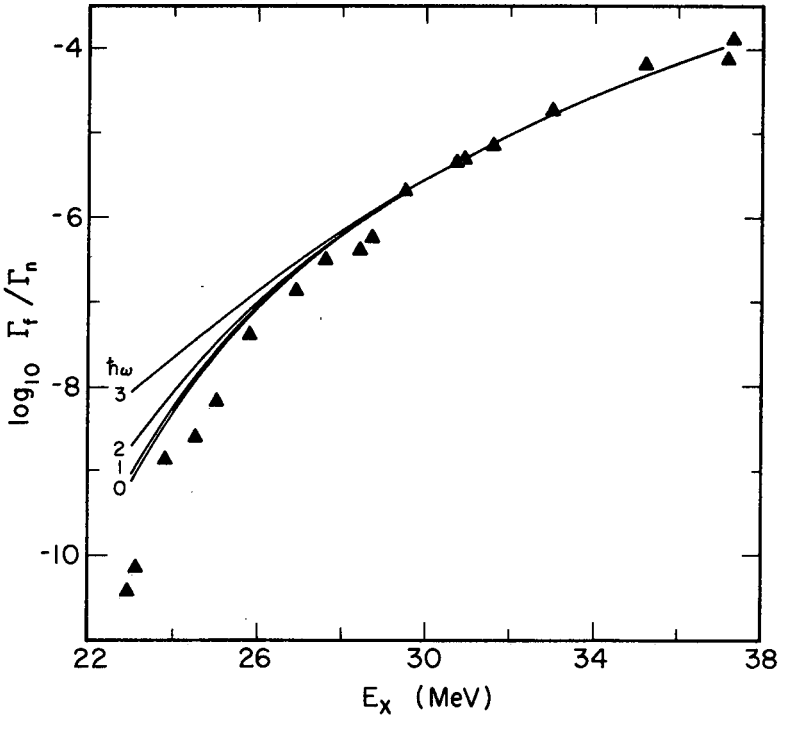
-4
-6
-8
-10
$\log_{10} \Gamma_f / \Gamma_n$
$\hbar\omega$
3
2
1
0
22
26
30
34
38
E_x (MeV)

MU-32971

$\hbar\omega$ (MeV)	B_f (MeV)	a_f (MeV^{-1})	a_n (MeV^{-1})	a_f/a_n
0	22.5	14.5	10.9	1.33
1	22.8	13.6	10.2	1.33
2	24.7	8.66	6.29	1.38
3	28.4	2.58	1.94	1.33

Fig. 9. The effect on $\log_{10} \Gamma_f/\Gamma_n$ of allowing three parameters, B_f, a_n, and a_f, to vary and fitting the measurements at 23, 30, and 37 MeV using various assumed values of $\hbar\omega$. The experimental points are indicated by triangles. Satisfactory fits to the measured data are obtained provided $\hbar\omega$ is not too large.

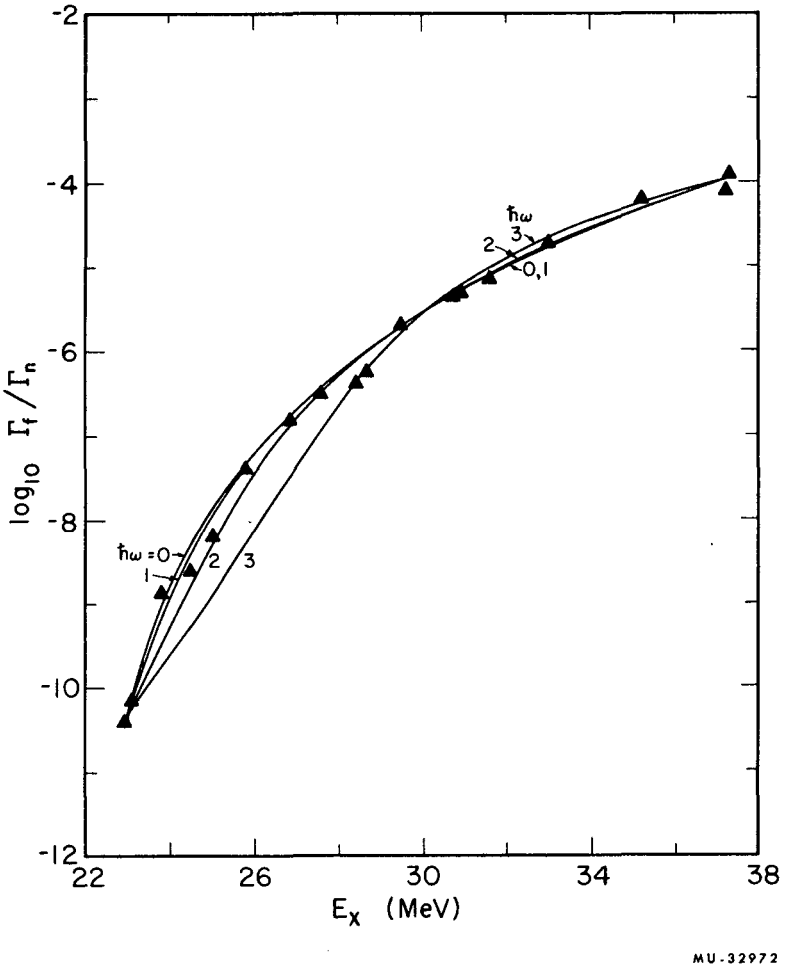
-2
-4
-6
-8
-10
-12
22
26
30
34
38
$\log_{10} \Gamma_f/\Gamma_n$
E_x (MeV)
$\hbar\omega$ = 0
1
2
3
$\hbar\omega$
3
2
0,1
MU-32972

$\hbar\omega$ (MeV)	B_f (MeV)	a_f (MeV^{-1})	a_n (MeV^{-1})	a_f/a_n	ψ^2
0	22.1	17.8	13.2	1.35	0.258
1	22.5	16.4	12.2	1.34	0.260
2	24.2	10.3	7.50	1.37	0.408
3	27.3	3.72	2.82	1.32	1.13

Fig. 10. Least-squares fits to the Γ_f/Γ_n data for a series of fixed values of $\hbar\omega$. The best fits are obtained for values of $\hbar\omega$ ranging from 0 to 1 MeV and B_f ranging from 22.1 to 22.5 MeV.

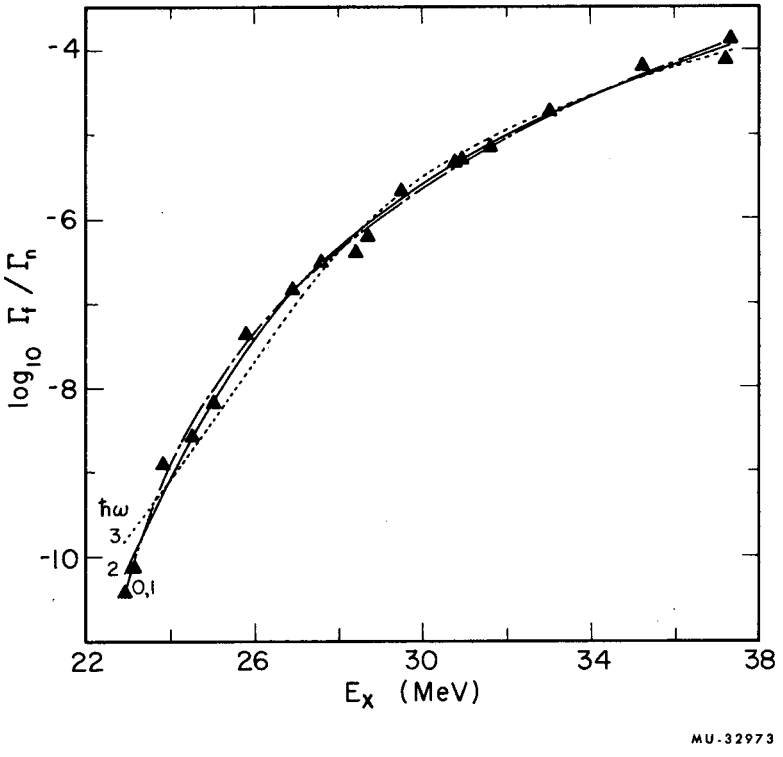
-4
-6
-8
-10
$\log_{10} \Gamma_f / \Gamma_n$
$\hbar\omega$
3
2
0,1
22
26
30
34
38
E_x (MeV)
MU-32973

$\hbar\omega$ (MeV)	B_f (MeV)	a_f (MeV^{-1})	a_n (MeV^{-1})	a_f/a_n	ψ^2
0.0	22.12	17.84	13.23	1.35	0.2583
0.4	22.17	17.86	13.27	1.35	0.2590
0.6	22.24	17.57	13.04	1.35	0.2595
0.8	22.35	17.06	12.64	1.35	0.2595
1.0	22.51	16.44	12.15	1.35	0.2599
1.2	22.71	15.65	11.53	1.36	0.2663
1.4	22.98	14.56	10.70	1.36	0.2768
1.6	23.32	13.36	9.76	1.37	0.3008
1.8	23.73	11.91	8.68	1.37	0.3439

Fig. 11. Least-squares fits to the measured data for various fixed values of $\hbar\omega$. Equally good fits may be obtained for any values of $\hbar\omega$ between 0 and 1 MeV. The effect of changing $\hbar\omega$ on B_f, a_f, and a_n can be seen in the accompanying table.

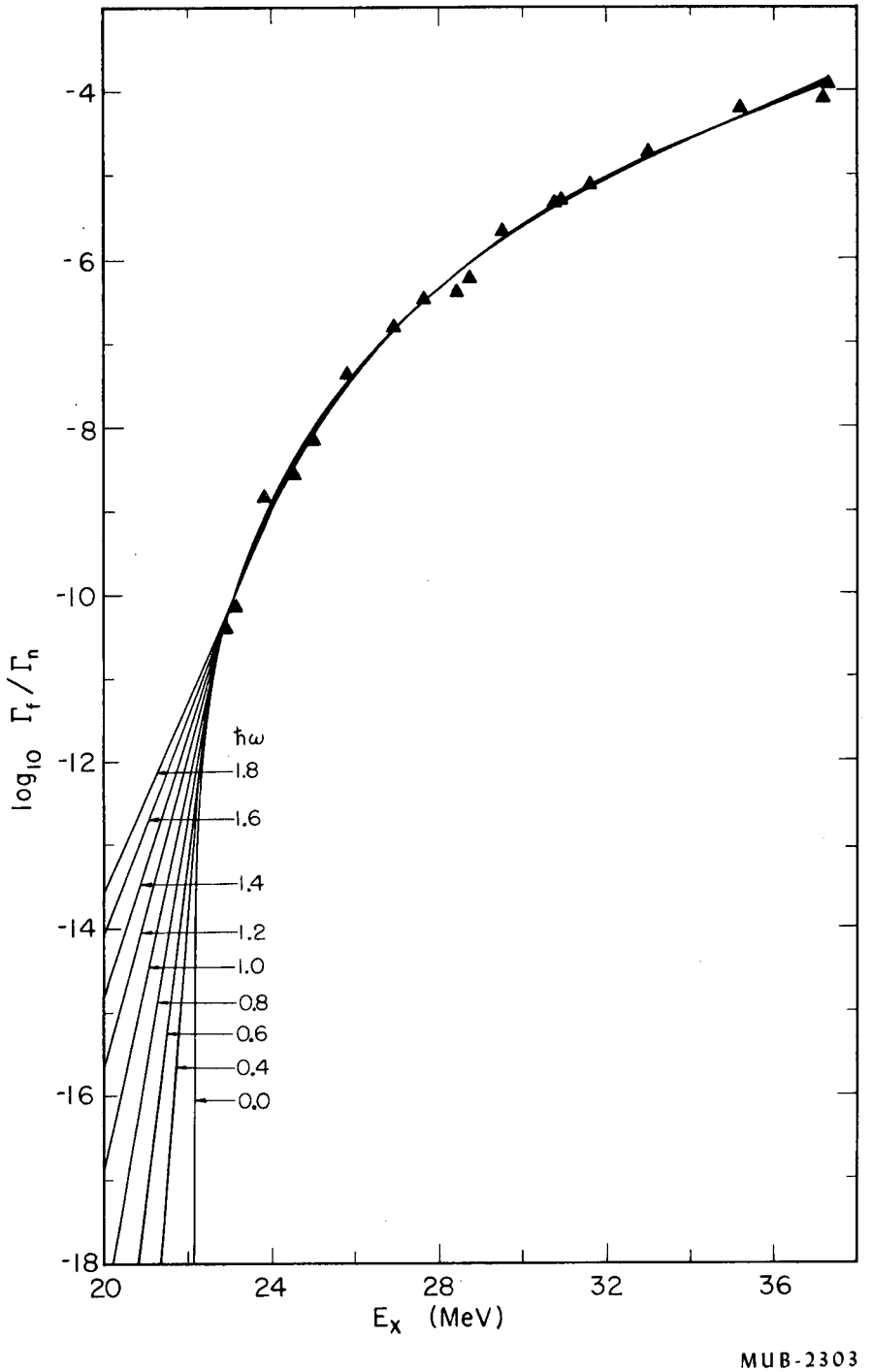
-4
-6
-8
-10
-12
-14
-16
-18
$\log_{10} \Gamma_f / \Gamma_n$
$\hbar\omega$
1.8
1.6
1.4
1.2
1.0
0.8
0.6
0.4
0.0
20
24
28
32
36
E_x (MeV)
MUB-2303

B_f (MeV)	$\hbar\omega$ (MeV)	a_f (MeV^{-1})	a_n (MeV^{-1})	a_f/a_n	ψ^2
18.0	0.00	79.6	61.9	1.29	1.59
19.0	0.00	57.4	43.5	1.32	1.29
20.0	0.00	41.1	30.5	1.35	0.955
21.0	0.00	28.8	21.1	1.36	0.579
22.0	0.00	18.9	14.0	1.35	0.266
22.5	0.978	16.4	12.2	1.34	0.260
22.6	1.08	16.0	11.8	1.36	0.264
22.7	1.17	15.6	11.5	1.36	0.266
22.8	1.25	15.2	11.2	1.36	0.269
22.9	1.32	14.8	10.9	1.36	0.273
23.0	1.38	14.3	10.6	1.35	0.277
24.0	1.85	10.6	7.79	1.36	0.367
25.0	2.20	7.63	5.64	1.35	0.518
26.0	2.51	5.40	4.06	1.33	0.738
27.0	2.82	3.73	2.90	1.29	1.01

Fig. 12. Least-squares fits to the measured data for various fixed values of B_f. The best fits as judged by the sum of the squares of the deviations are found in the neighborhood of B_f = 22 or 23 MeV, with $\hbar\omega$ between 0 and 1.4. The corresponding range of values of the pair a_f, a_n is between 18.9,14.0 and 14.3,10.6 MeV^{-1}.

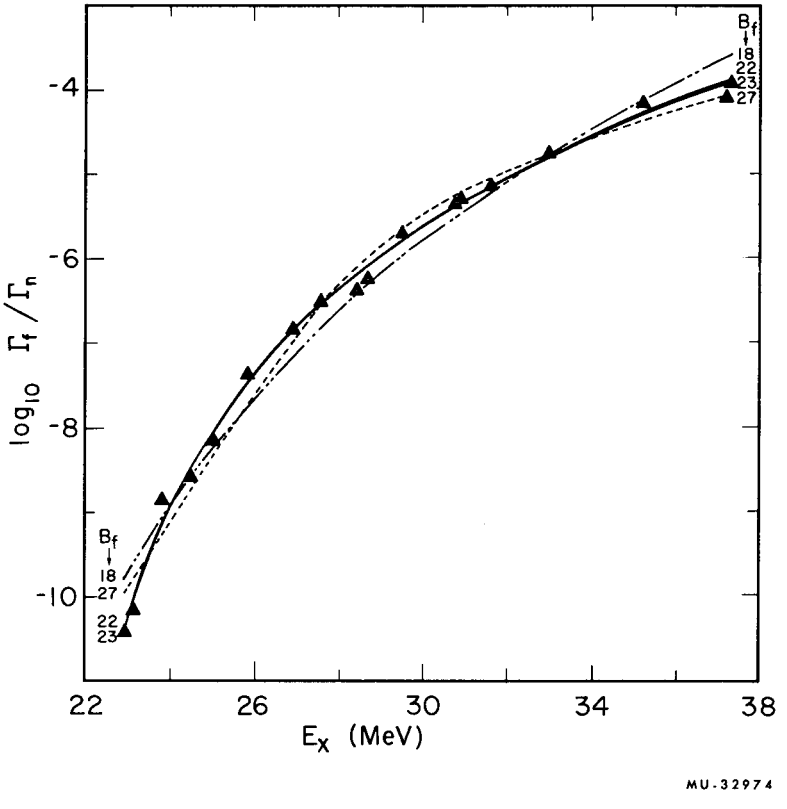
B_f
18
22
23
27
-4
-6
-8
-10
$\log_{10} \Gamma_f / \Gamma_n$
22
26
30
34
38
E_x (MeV)
MU-32974